Acta Astronautica 203 (2023) 146–156

Contents lists available at ScienceDirect

Acta Astronautica

journal homepage: www.elsevier.com/locate/actaastro

Research paper

Implicit lunar dust mitigation technology: Compliant mechanisms

Dorota Budzyń [a,*], Hossein Zare-Behtash [a], Aidan Cowley [b], Andrea Cammarano [a]

[a] James Watt School of Engineering, University of Glasgow, 1 University Ave, Glasgow, G12 8QQ, United Kingdom
[b] European Astronaut Centre, European Space Agency (ESA), Linder Hoehe, Cologne, 51147, Germany

ARTICLE INFO

Keywords:
Lunar dust
Dust mitigation
Compliant mechanisms
Mechanisms design

ABSTRACT

The finest fraction of the lunar regolith, namely the lunar dust, poses a challenge for hardware design and lunar operations. The Apollo missions experienced equipment malfunctions and failures due to dust interactions with hardware. In this work we focus on the problems related to the clogging of rigid body mechanisms. We explain the causes of the problem and propose a solution consisting of replacing traditional mechanisms with compliant mechanisms. There are multiple methods for synthesizing compliant mechanisms, but two approaches are most commonly used: analytical design and topology optimization. In this paper using a compliant gripper as an example, the suitability of these methods to design compliant mechanisms used in extra-vehicular activities is investigated. In doing so, the feasibility of using complaint mechanisms in the lunar equipment as part of dust mitigation strategies for surface projects is also demonstrated.

1. Introduction

The Apollo missions, the only crewed lunar missions performed so far, provided an enormous amount of data about the Moon. Several findings highlighted the challenging nature of interactions between the Apollo hardware and the lunar environment. One of the aspects which had a substantial impact on hardware operations was lunar dust. Lunar dust is the fine fraction of lunar regolith. Between 10% and 20% of lunar regolith weight consists of particles smaller than 20 μm [1]. During the Apollo operations, particles smaller than 2 μm proved to be the most problematic [2]. The fragments of this size are able to enter hardware gaps, clearances and backlashes between hardware elements, causing the increase of friction and decrease of performance. The dust particles were created by meteorite impacts and were never exposed to hydrological or aeolian erosion, hence they retain very sharp edges. Furthermore, the minerals present in the dust, such as anorthite, bytownite, labradorite, fayalite or forsterite, score 6 and above on the Mohs scale of minerals hardness [3]. As for comparison, most steel alloys score 4–4.5 on the same scale. This means that the engineering materials of the hardware are exposed to sharp particles consisting of harder materials, leading to the risk of abrasive wear [4].

Dust contamination probability is high as a result of lunar dust particles periodically floating above the surface due to electrostatic phenomena [5]. New studies estimate that floating particles can concentrate around 2 m above the Lunar surface, while the photoelectron sheet extends to tens of meters [6]. The lofted dust is particularly significant in the terminator regions (during sunset and sunrise). The Sun-facing side of the Moon is exposed to solar wind plasma, free electrons, and solar UV rays which cause photoemission [7,8]. This creates a plasma sheath of photoelectrons above the day-side of the surface. As a result, the day side of the surface charges to positive potentials. The opposite (night) side sheath is dominated by positive ions that can extend to 1 km above the ground and the surface charges to negative potentials [9,10]. The exact potential of lunar dust particles depends on the work function of the surface (energy needed for extraction of an electron from the surface). Previous work has determined the work function of the lunar regolith to be around 5.8 eV [11]. The work function of engineering materials often used in space hardware is usually different than the one of lunar dust, e.g. aluminum 4.28 eV, stainless steel 4.4 eV. Therefore hardware and lunar dust particles charge to different potentials. Usually, in order to get the dust off the surfaces, brushes are used. They rely on breaking the bonds induced by the van der Waals forces, but the electrostatic forces are much stronger and harder to break. The potential difference is the main reasons for the adhesion of the dust particles to the hardware surfaces. This is also the reason why cleaning of the hardware with mechanical methods, like brushes during Apollo missions, was harder than expected [5].

Several dust mitigation technologies including coatings, electrostatic discharge films, work function matching, brushing, blowing, electrodynamic methods, vibration, ultrasonic techniques have been investigated in the literature as dust mitigation solutions for the lunar environment [5,12]. The appropriate protection method for each case must take into account the type of expected damage. Based on the

* Corresponding author.
E-mail address: d.budzyn.1@research.gla.ac.uk (D. Budzyń).

https://doi.org/10.1016/j.actaastro.2022.11.042
Received 20 September 2022; Received in revised form 27 October 2022; Accepted 22 November 2022
Available online 24 November 2022

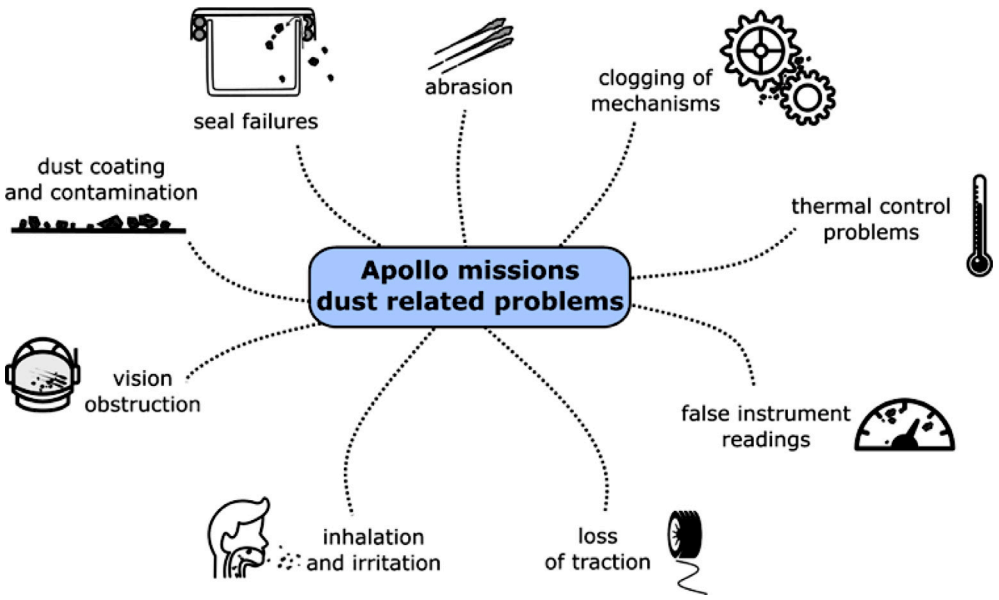

Fig. 1. Apollo dust related problems chart, based on categorization from Gaier et al. [13].

Fig. 2. Apollo Lunar Sample Return Container (ALSRC) from Apollo 11 mission [14], hinges highlighted with red dashed outlines.

Table 1
Apollo mechanisms dust-related problems based on the astronaut de-briefings [13].

Mission	Problem
Apollo 12	Lock buttons of the equipment conveyor very hard to manipulate because of the dust accumulation in the moving parts
Apollo 15	Camera drive mechanisms got jammed with dust and prevented it from working
Apollo 16	Battery cover of radiator jammed because of dust accumulation in the mechanism
Apollo 17	Some of the moving components of the geopallet got stuck after the second EVA; the angle adjustment of some geological tools (scoop and rake) got fixed in one position which could not be changed anymore; multiple components attached to the rover jammed because of the dust exposure (e.g. bag holders, pallet locks)

reports of the Apollo surface missions, the dust related problems were categorized into nine groups [13]. This classification is presented in Fig. 1.

This work focuses on one specific category of problems: clogging of mechanisms. Mechanisms present in the Apollo surface equipment that suffered from dust damage were build as rigid-body mechanisms. Rigid-body mechanisms consist of stiff elements connected by kinematic pairs (hinges, sliders etc.). An example of such a mechanism is an opening mechanism of a sample container that has a hinge attached to the lid. Fig. 2 shows Apollo sample container with highlighted hinges. The process of dust related damage propagation for such mechanisms starts with the contamination. The dust particles enter the backlashes (gaps) in the mechanism, increasing the friction in the mechanism and, therefore, the energy required for operations. Prolonged accumulation of dust further increases the friction in the mechanism, which ultimately leads to jamming. Some examples of dust-related damage of mechanisms mentioned in the Apollo de-briefing reports and discussed in the literature are presented in Table 1.

The common cause of these problems is the exposure of the gaps between adjacent sliding or rolling elements in the mechanisms to lunar dust. Due to the electrostatic phenomena causing the dust to move above the lunar surface, dust protection by exposure avoidance is challenging. Hence, this work evaluates a novel approach for the design of Extravehicular Activity (EVA) equipment. The proposed solution is to use an alternative design methodology where all the inter-element gaps are eliminated, and traditional mechanisms are replaced with compliant mechanisms. The lack of inter-element gaps makes compliant mechanisms resilient to jamming caused by lunar dust: this approach can be categorized as an implicit dust mitigation technology complementary to already well established active and passive dust mitigation technologies [12]. It is important to note that there is no single dust mitigation technology that can solve all dust induced problems [5]. Nonetheless, complaint mechanisms, used as a replacement of rigid-body mechanisms, can eliminate the wear and performance decline associated with increased friction and jamming. Furthermore, compliant mechanisms can be designed and manufactured as monolithic pieces and are good candidates for additive manufacturing: this is in line with ESA's interest of in-space manufacturing.

The use of compliant mechanisms in space, to date, is limited. Although some notable examples of compliant pointing mechanisms and large-angle flexure pivot were proposed in the literature [15–17], they have not been included in any space mission yet. The compliant mechanisms used in the space hardware today are usually located in scientific payloads as presented in the literature [18–24]. The application of flexures usually in conjunction with traditional mechanisms can

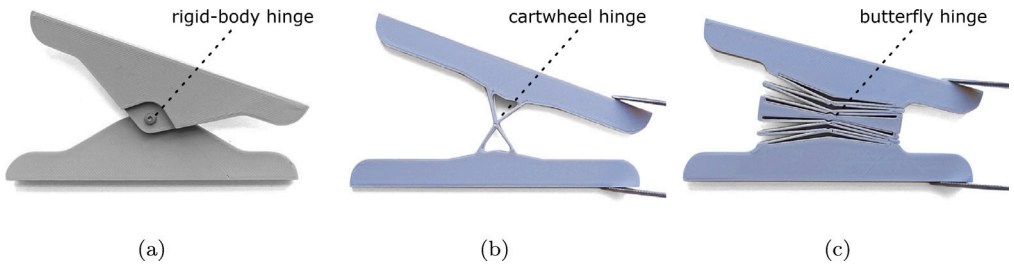

Fig. 3. Rigid body hinge (a), and various designs of compliant hinges (b) and (c).

increase the precision while enhancing volume reduction. Moreover, to the best of the knowledge of the authors, there has been no reported work looking into the design of 3D printed lunar surface EVA hardware featuring compliant mechanisms for dust mitigation. This is a novel method of dust protection from wear of mechanical kinematic pairs which usually leads to increased friction and jamming. The implicit dust mitigation methodology proposed here can be directly included in the design process of hardware development and minimize the post manufacturing enhancements (coatings, seals etc.). This paper explores the feasibility of using such an approach and demonstrates that compliant mechanisms can be a viable option to develop dust resilient EVA equipment for the future lunar missions.

2. Design methodology for compliant mechanisms

Rigid-body mechanisms require multiple components connected by kinematic pairs to achieve motion, whereas in compliant mechanisms this can be done with a single component. This brings great advantages from a manufacturing perspective: compliant mechanisms can be designed and fabricated as monolithic pieces, reducing assembly times and costs. In compliant mechanisms elastic deflection is used to obtain motion, avoiding inter-element friction, reducing tribological wear, eliminating the need for lubrication and reducing maintenance [25–27]. The effectiveness of lubrication in space tends to diminish over time due to evaporation of liquid lubricants and surface wear of dry lubricants [28]. Slow degradation of lubrication has a detrimental impact on the operations of the mechanism, affects its precision and reduces the lifetime of the mechanism. Complaint mechanisms do not need lubrication and therefore are immune to this problem. Furthermore, they are suitable candidates for high precision applications [29–31].

An example of conventional rigid body hinge compared to compliant hinge designs is presented in Fig. 3. The input work supplied to a compliant mechanism is partially stored as elastic energy in the material, and once the input is removed the mechanism can spring back to its original shape. This makes compliant mechanisms particularly well suited to replace traditional spring loaded mechanisms. As such, compliant mechanisms with localized compliance, visible as flexures (thin material areas), can be modeled as rigid body hinges with torsion springs applied in each joint (to mimic the elastic energy stored in the compliant hinge). This method can be used for designing complaint mechanisms and is known as the Pseudo-Rigid-Body method [32].

From the topology synthesis point of view, designing compliant mechanisms is more challenging than designing rigid body mechanisms, especially when compliant mechanisms with intricate designs are necessary. To reduce complexity, various analytical methods have been developed. A high-level overview of these methods can be found in Fig. 4. The works of Howell et al. [25] and Hopkins and Culpepper [33] detail the capabilities and limitations of such methods. Analytical methods have the advantage of being more intuitive to those who are familiar with designing rigid body mechanisms. The first subgroup of analytical methods – Rigid Body Replacement Method (RBRM) [32] – replaces hinges and other kinematic pairs with compliant hinges and flexures. This approach relies on the existence of an initial rigid body design. The final shape is typically very similar to the original design and excludes potentially more effective solutions that would require larger portions of the mechanism to be compliant.

Two additional analytical methods – Freedom And Constraint Topology (FACT) [33] and Building Blocks Approach [34] – use libraries of compliant elements or sub-mechanisms to achieve relative displacement with one or more compliant elements that together fulfill the desired kinematic function. This can be a very effective design approach because it follows similar steps to designing rigid body mechanisms. Overall, the existing analytical design methods show good potential and can help to synthesize solutions in an effective and fast way while giving the designer a great deal of flexibility in terms of sub-mechanism selection. In Section 3.2 an example of the design obtained using the analytical method from the Building Blocks Approach will be presented.

Several works propose the use of topology optimization as an alternative design approach for compliant mechanisms. Topology optimization is a method that aims at identifying the optimal material distribution for given boundary conditions [35]. The problem is formulated in terms of an objective function and design constraints. In static structure optimization, topology optimization aims at maximizing stiffness. This can be achieved directly by maximizing the stiffness or indirectly by minimizing displacement or compliance. For a model with prescribed loads this results in considerably stiff structures. Common design constraints are volume fraction, mass fraction or total mass. Topology optimization capabilities for static structures are available in commercial mechanical design software packages. However, topology optimization for compliant mechanisms in commercial software is in its early stages and is less user friendly when compared to static structures topology optimization.

Intuitively, when designing a flexible element the designer is tempted to maximize compliance in order to enhance flexible displacements. However, this approach is far from ideal: if maximum compliance is sought, this would result in a design that contains mostly void space. This is due to the fact that in all commercial software packages for topology optimization known to the authors void spaces do not have zero Young's modulus. For numerical stability, it is necessary to set the Young's modulus of void spaces to a very low value. As such, empty design domains have very low stiffness and solvers could still present them as viable outcome topologies. Furthermore, forcefully maximizing the compliance could also result in areas where some material is disconnected from the rest of the mechanism (in reality it is connected through voids or material with low densities and Young's modulus). Finally, by simply focusing on compliance, one can overlook important design requirements. For example while designing a compliant gripper it is desirable for the gripper to be flexible enough to deflect in response to the input of the operator but also stiff enough to grab and hold the target object [36]. The need to balance stiffness and compliance under specific conditions complicates the formulation of the objective function for complaint mechanisms.

Saxena and Ananthasuresh [36] explored several formulations of the compliant mechanism objective function. The formulations presented there are a combination of Mutual Potential Energy (MPE) and Strain Energy (SE). Other notable formulations from the literature include Geometric Advantage (GA), Mechanical Advantage (MA) and Mechanical Efficiency (ME) [37]. To date, a standard best practice

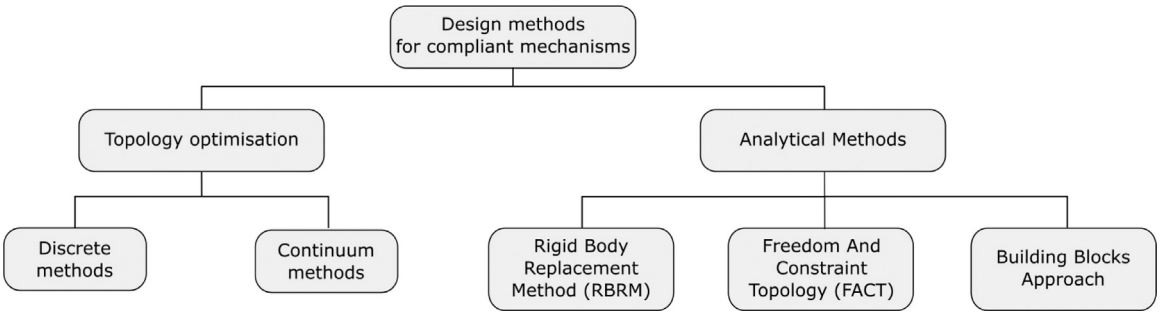

Fig. 4. Design methods used to synthesize compliant mechanisms.

formulation approach has yet to be identified. Furthermore, different objective functions for topology optimization of compliant mechanisms tend to result in similar topologies [38]. In the majority of formulations, additional boundary conditions are typically applied to the output and/or input node of the mechanism. Those additional boundary conditions are represented as restoring forces from springs with stiffness constants k_{in} and k_{out}. More details on this topic can be found in the works from Bendsoe and Sigmund [39], Ansola et al. [40] and Cao et al. [41]. The selection of appropriate spring stiffness values can pose a challenge. Inappropriate selection of external spring stiffness can cause problems with convergence of the solution or result in a final topology with voids between input and output. Existing literature provides useful guidelines on the selection of such stiffness values [37].

The approaches for topology optimization mentioned above are often used in MatLab scripts and are not always easily transferable to commercial software. Furthermore, such formulations are force driven. As an alternative, a simple and versatile topology optimization formulation for flexure synthesis has been presented by Koppen et al. [42]. The aforementioned work focuses on a formulation meant to satisfy short-stroke flexure design and it is displacement driven. It focuses on strain energy under prescribed displacements and, since it is meant to be used with small displacements, it assumes a linear stress–strain relationship. This formulation can be used in conjunction with commercial software — in this work it is used with HyperWorks.

The methodology of Koppen et al. [42] used for flexure design uses multiple loading cases — one to maximize stiffness in the direction opposite to desired movement (also referred to as degree of constraint), and another to define maximum stiffness (or compliance) for a loading case with the desirable deflection behavior (degree of freedom). The load cases are defined using prescribed displacements rather than forces which is the reason why compliance and stiffness are proportional, unlike in force driven designs (where compliance is the inverse of stiffness). This point is further investigated in [43,44] where the load versus displacement driven optimization is explored. In this work, the presented mechanisms synthesis is displacement driven and therefore, like in the work of Koppen et al. [42], maximizing the compliance (or strain energy) leads to the maximization of stiffness. Here, this method is adopted to synthesize a compliant mechanism, namely the compliant gripper presented in Section 3.1.

3. Case study: lunar gripper

Selected approaches discussed in the previous section are applied to an example mechanism, demonstrating the feasibility of replacing rigid-body mechanisms in lunar hardware with compliant mechanisms. One of the geological tools from the Apollo program, namely the Tongs, is here reproduced using compliant mechanisms. This has been a critical tool for the Apollo missions since the astronauts' spacesuits did not provide enough dexterity to allow them to pick up rock samples from the ground without any tools. The Tongs were used to collect rock samples with diameters smaller than 10 cm [45]. Fig. 5 presents astronaut Charles Conrad Jr. using the tool to pick up a rock sample on

Fig. 5. Tongs used by astronaut Charles Conrad Jr. during the Apollo 12 mission [47].

the lunar surface. This geological tool was one of the most successful tools and was the only one present in every surface Apollo mission [46] (see Fig. 6, taken by the authors). The kinematic behavior of the Tongs was quite simple: the mechanism was spring-loaded, by pulling the T-bar handle the astronaut could open the jaws of the Tongs and by releasing the handle the jaws were closing. In the default position, the jaws were closed as shown in Fig. 6. The position of the output (the jaws) was determined by the position of the input (the handle), therefore for the present discussion the design of this mechanism is displacement driven.

Since a compliant mechanisms will store elastic energy when deformed, no spring-loading is needed. It is also likely that achieving large displacements might be more challenging for compliant mechanisms than for rigid-body mechanisms of similar size. That is why, it is assumed that the default position of the gripper is not closed, but open, to extend the range of motion. Usually compliant mechanisms have limited motion range therefore, to achieve larger range, although the gripper's equilibrium position is open, the compliant Tongs are designed to be able to open even further. The direction of input displacements will determine if the gripper will close or open its jaws: the mechanism is designed to exhibit output motion mainly in the horizontal direction in Fig. 7, where a conceptual model of such gripper is presented. In Fig. 7 a representation of the pulling input force (jaws opened) and pushing input force (jaws closed) is provided. Compliant mechanisms present a good aptitude to scalability [48] and for this demonstration a compliant mechanism smaller than the Apollo Tongs is selected. The gripper designs presented here can grasp objects up to 4 cm wide, which is around half the size of the samples collected by the Apollo Tongs. The designs presented here can be easily re-scaled to

Fig. 6. The training replica of Apollo Tongs, photographed in ESA's European Astronaut Centre.

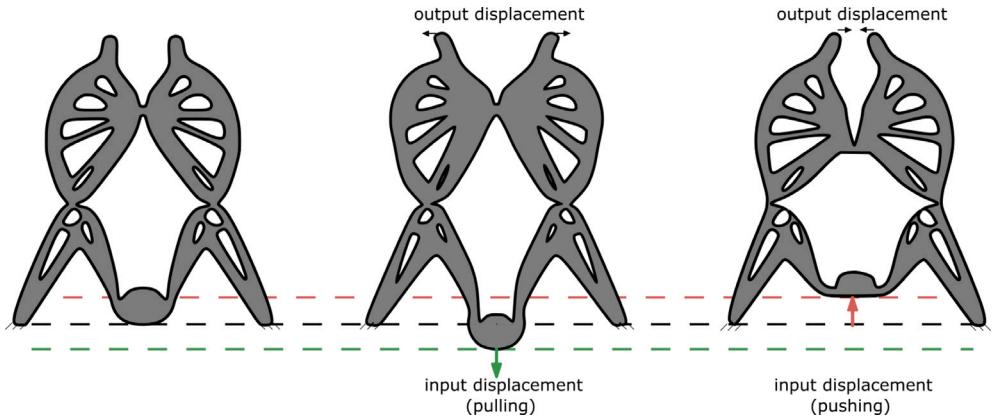

Fig. 7. Functionality of complaint gripper. From left to right: pulling on the input – opening the gripper, default gripper position, pushing on the input – closing the gripper.

the size of Tongs, but to facilitate the manufacturing and experimental campaign in Sections 3.1 and 3.2, in this work only the scaled version will be considered.

As discussed in Section 2 multiple approaches to design complaint mechanisms exist: here the methodology to design the compliant gripper following the *instant center approach* (analytical method) and *topology optimization* are presented, highlighting the difference between the two approaches and assessing the performance of the resulting designs.

3.1. Topology optimization of compliant gripper

The design presented in this section utilizes *topology optimization* and the two loading cases method described in Section 2. The problem was formulated using the commercial software HyperWorks OptiStruct. The gripper was designed using material parameters of Thermoplastic Co-Polyesters (TPC). It has been selected for its availability for 3D printing and fast prototyping. It is a good rapid prototyping alternative to the other flexible material that was used in the Apollo equipment — fluorosilicone [45]. The expected mechanism volume was set to 40% of the design domain. The input–output behavior was already discussed in Section 3. As shown in Fig. 8, half of the gripper is modeled (assuming its symmetry); the input force is located at the top left corner of the design domain and the output point is expected to be at the right edge of the domain. In this formulation of the topology optimization, a GA is indirectly selected while defining the prescribed displacements. Assuming that the base requirement is that the input displacement is comparable to the output displacement, the optimization is initiated with a target GA of 1 (i.e., input displacement equal output displacement). For sake of simplicity here a unitary input displacement is considered. The design has been developed considering the following boundary conditions: bottom left corner fixed; top edge free in the horizontal direction and constrained in the vertical direction.

Optimization objectives and optimization constraints are presented in Table 2. The mechanism needs to be compliant enough to support the deformation defined by loading condition 1 (expected displacements) and stiff enough in the opposite direction — defined as load case 2. The objective for the optimization process is maximizing the stiffness of load case 2. It is important to note that for force driven designs compliance is the inverse of stiffness. As the mechanism design is displacement driven, the stiffness is proportional to both compliance and strain energy. The difference in the compliance vs. stiffness relationship for force and displacement driven designs is explained in the user manual of the HyperWorks OptiStruct software version 2022 [49]. In the case of the design presented in this work, compliance is maximized as an objective of the optimization process. There are also two optimization constraints in this procedure. The first one is based on load case 1, which ensures enough flexibility and therefore constrains the stiffness — here equivalent to compliance. The compliance of the design for load case 1 shall be smaller than the defined upper bound (here 0.1 N mm). Finding the appropriate upper bound is dependent on the material and users should scope various values to select one that yields satisfactory results. If the value is too large the mechanism will behave almost like a static structure (not capable of deformation), and if it is too small the simulations may encounter convergence problems or generate results with very localized flexure hinges and/or intermediate densities. The last optimization constraint assumes maximum volume fraction: this constraint is defined for the whole design domain and is not specifically linked to any load cases.

Table 2
Summary of objective and constraints applied to the modeled load cases.

	Load case	
	1	2
Objective	–	Maximize compliance
Constraints	Compliance $\leq$ 0.1 N mm Volume fraction $\leq$ 0.4	–

Fig. 9 shows the summary of evolution of the design during the simulation that was run for 50 iterations. The maximum limit of iterations for this simulation was set to 100, but the simulation reached the software convergence criterion after 50 iterations and therefore stopped. In HyperWorks the default convergence criterion is based on the relative change in the objective function. If between two design iterations the change in objective function is less than 0.5%, then the optimization stops. The volume constraint has been set to a value of 40% therefore the design process starts with a material density equal to 0.4 times the density of TPC material (pseudo density = 0.4). The software used utilizes the SIMP method (Solid Isotropic Material with

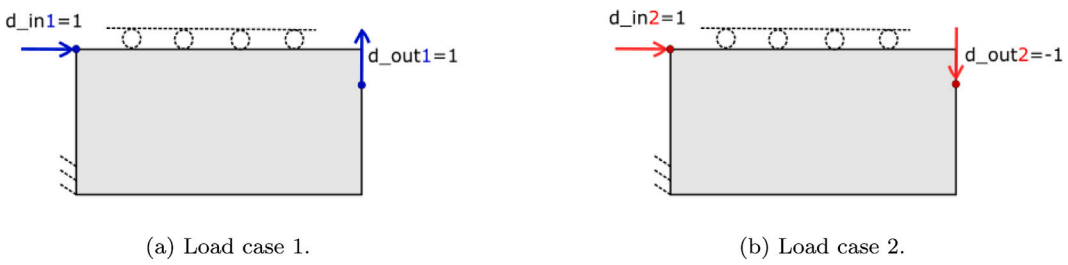

(a) Load case 1. (b) Load case 2.

Fig. 8. Load cases and the design domain of compliant gripper for topology optimization.

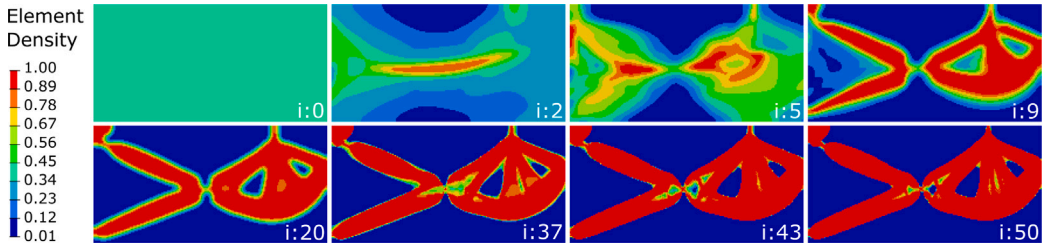

Fig. 9. Topology optimization compliant gripper evolution of density color map, i - number of iteration (starting with 0). (For interpretation of the references to color in this figure legend, the reader is referred to the web version of this article.)

Fig. 10. Optimized compliant gripper 3D printed with TPC.

Penalization). In this method pseudo density is the design variable. The pseudo density value can have any value greater than zero and smaller or equal to one. This method uses power penalization to morph elements into one of the desired states (void – approaching zero and solid – approaching one). The stiffness of each element in the design domain is a function of penalized pseudo density multiplied by the stiffness of the design material. More details about the methodology can be found in literature [39,50,51]. In the context of manufacturing the pseudo densities do not have a good physical representation, i.e., elements of density below one should have mechanical properties that scale down with the pseudo density. In reality, when 3D printing with lower infill this requirement is not satisfied because the stiffness is not proportional to the infill. In the last iteration of the topology optimization intermediate pseudo densities are present — see Fig. 9. Since it is impossible to manufacture intermediate densities appropriately, a binary approach has been adopted where pseudo densities below 0.75 have been filtered out and replaced with voids and pseudo densities equal and above 0.75 have been replaced with full density TPC. The threshold value is generally chosen by the designer to maintain a good balance between ensuring that all the parts of the design are connected – if the threshold is too high design can split into multiple components not connected to each other – and the compliance of the flexures is preserved — if the threshold is too low, more material is added to the flexures, which increases their stiffness. The final design was also equipped with mounting holes and gripper claws. The 3D printed gripper is visible in Fig. 10.

To demonstrate the kinematic behavior of the grippers displacement driven tests were conducted. The input of the gripper was connected to the linear displacement screw-nut mechanism. Such an input would not be a suitable mechanism to be used on the Moon, but the selection of a suitable drive is outside of the scope of this work. The input mechanism of this type was selected as it is cost-effective, and provides reliable positioning and accuracy. The output displacement values are determined by Digital Image Correlation (DIC). The software used for image post-processing was the openly available ImageJ.

The measurements from the deformation tests are presented in Fig. 11. The data is marked in red when pushing - which results in the output ports to come closer together and the jaws of the gripper to close, and in blue when pulling - moving the output ports further away from each other. The standard deviation of the measurements is relatively small and therefore cannot be presented in the figure. The maximum standard deviation calculated for data presented in Fig. 11(a) equals 0.22 mm. The slope of the linear regression in the same figure provides a measurement of the GA, i.e. the ratio between output displacement in the desired direction (here horizontal: d_{outX}) to the input displacement (d_{in}). An achieved GA value of 1.479 is higher than a GA equal to 1 which was a result of initial boundary conditions (displacements). Obtaining a certain GA is not an objective of topology optimization methodology presented here, and the difference is not an unusual development. Achieving a GA value higher than the one resulting from prescribed displacements, in this case, is desirable as the input displacement required to achieve the same output range decreases. Fig. 11(b) shows the motion path of the output port located on the right jaw of the gripper - the coordinate frame is marked in the same sub-figure. This point is also a center point for the measurements, which means that the gripper closure results in negative values along x-axis. Maximum standard deviation for the data presented in Fig. 11(b) equals 0.72 mm in X direction and 0.48 mm in Y direction. It is visible from Fig. 11(b), that the output port exhibits both horizontal and vertical movement. The range of y-motion is equal to 36% of the motion in the x-direction. Although the desired motion is only in the horizontal direction no constraint has been applied to limit the vertical motion: this is to provide a fair comparison with the analytical design presented in the next section. It is fair to say that any vertical movement can be considered as a reduction in efficiency, nonetheless the expected horizontal movement is dominant.

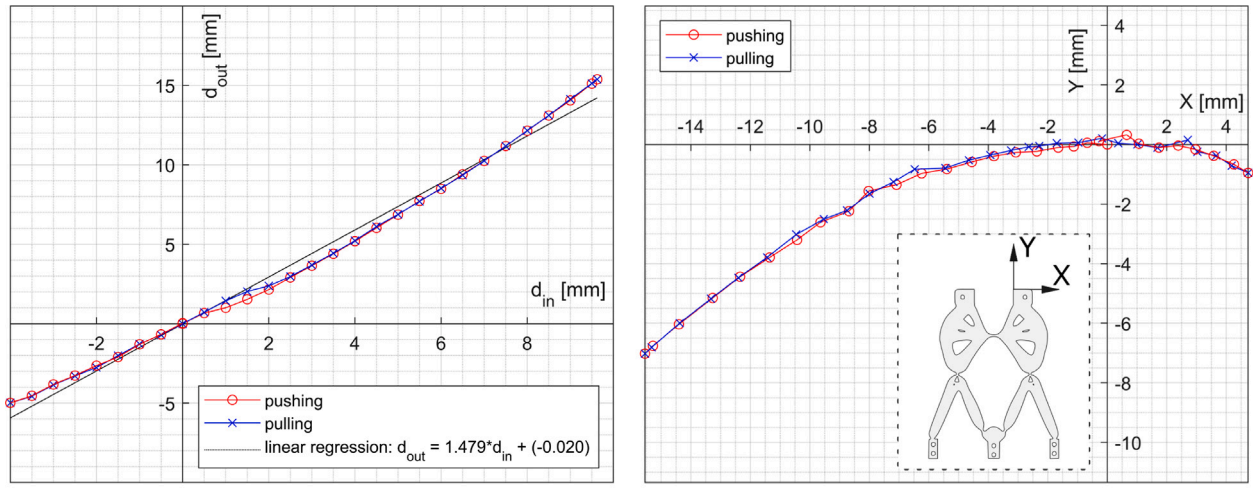

(a) Displacements relationship. (b) Output port motion path.

Fig. 11. TPC gripper kinematic behavior; graphs based on three tests and the mean of measured values; d_{in} - input displacement; d_{out} - output displacement. (For interpretation of the references to color in this figure legend, the reader is referred to the web version of this article.)

(a) Default position. (b) Open position. (c) Close position.

Fig. 12. Various deflection stages of the TPC gripper with undeformed blue shape visible in the background. (For interpretation of the references to color in this figure legend, the reader is referred to the web version of this article.)

Fig. 12 presents three different stages of the TPC gripper deformation: unreformed, open and close. The blue shade in the background represents the undeformed gripper and showing that the desired kinematic behavior was achieved.

3.2. Analytical compliant gripper design

In this section the *instant center approach* is utilized to obtained a design of a compliant gripper. More details on this method and its use can be found in [52].

Fig. 13 shows the design steps taken to synthesize the final design presented in Fig. 14. The first step shows the definition of the design domain (gray) including the input and output points with their desired input displacement d_{in} and output displacement d_{out}. In the second step, dashed lines are added, perpendicular to the expected input and output displacements directions. These lines determine the position of flexures to be added in the last design step. An ancillary point is then selected with an arrow showing the direction of movement of the selected point, this is marked with a blue 'X' in Fig. 13. The rules for the selection of this point and its direction are not well defined and mostly rely on the experience of the designer. Here a point close to the outer perimeter of the design domain has been selected to maximize the length of the flexures, minimize the stress, and maximize the displacement. A line is drawn perpendicular to the direction of movement (blue fine-dotted line) through this point, this line crosses the previous dashed lines producing two additional points - they are the centers of rotations of the "building blocks" of the design. The last step involves filling this geometry with design elements (in green in the final step). Here, the triangular elements provide rigidity to the mechanism whereas the thin long green elements are flexures and act as compliant elements.

This method does not require to define specific GA value at the design stage and therefore the resulting GA will differ from the one obtained in topology optimized gripper. Nonetheless, the geometry is quite simple and therefore it is easy to analytically determine the Geometric Advantage (GA) once the geometry is sketched. GA is the ratio between the output and the input displacement and depends on the distances between input (P_{in}), output (P_{out}), the ancillary point (X) and centers of rotation (R_1 and R_2) as shown in Fig. 14(a). The polylactic acid (PLA) 3D printed gripper prototype is presented in

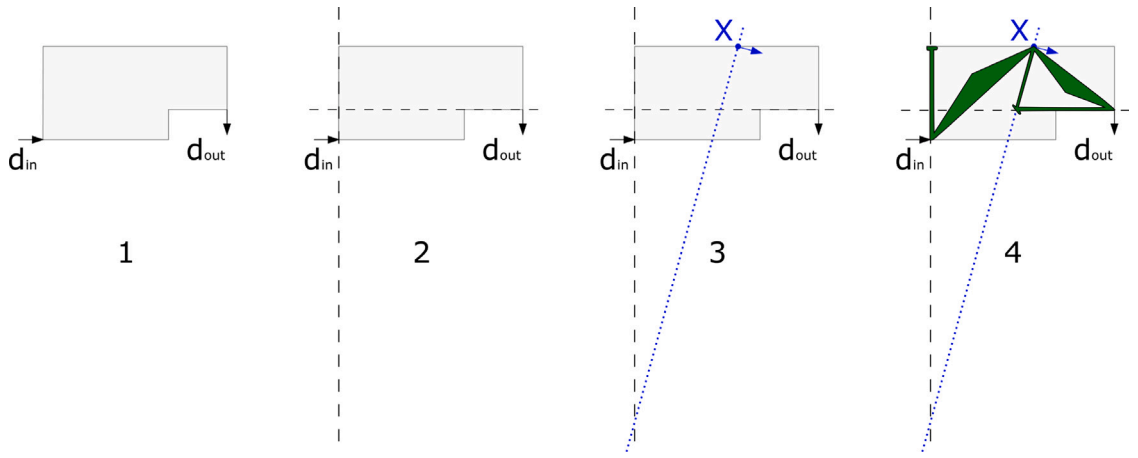

Fig. 13. Design steps of the instant center approach for a compliant gripper design. (For interpretation of the references to color in this figure legend, the reader is referred to the web version of this article.)

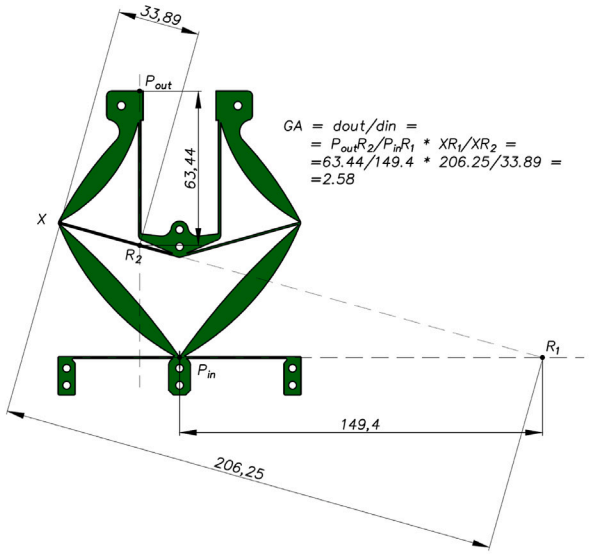

(a) PLA compliant gripper model; green - final design outline, black - measurements and calculations needed to determine expected Geometric Advantage (units: mm).

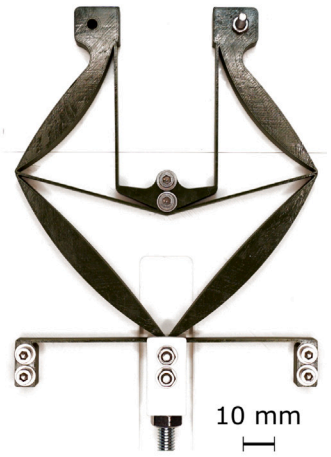

(b) Compliant gripper 3D printed with PLA.

Fig. 14. PLA compliant gripper. (For interpretation of the references to color in this figure legend, the reader is referred to the web version of this article.)

Fig. 14(b). PLA was selected for its ease of use with additive manufacturing technologies. Furthermore, PLA based composite materials enriched with lunar regolith particles are now under development in several research groups [53,54].

The displacement tests performed on this gripper are the same as for the previous design. The resulting displacements are presented in Fig. 15. Similarly to previously discussed tests of topology optimized gripper, the input displacement is marked in red when pushing and in blue when pulling on the gripper input. Maximum standard deviation for data presented in Fig. 15(a) equals 0.22 mm. In Fig. 15(a), it can be observed that around 1 mm of input displacement hysteresis is present. Nevertheless, the remaining part of the curve indicates a linear relationship. The linear regression gives a value of GA of 2.573 which is comparable to the value of 2.58 calculated using the distances from the center of rotations as discussed above. Fig. 15(b) displays the motion path of the output port located on the top right - coordinate system marked on the undeformed gripper in the same figure. Maximum standard deviation for values in X direction equals 0.49 mm and for Y direction 0.62 mm. It is visible that the horizontal direction is dominant, as was intended at design stage. The paths for closing and opening the gripper are very close to one another. The different stages of the gripper deformation are presented in Fig. 16 with the blue shade representing the undeformed (unloaded) gripper in the background.

4. Conclusions

Lunar dust poses a challenge for surface hardware design. In this paper we propose the application of compliant mechanisms as an implicit dust mitigation technology that eliminates the dust-sensitive aspects of equipment, specifically rigid-body mechanisms prone to jamming. The compliant mechanisms are free of inter-element friction and therefore can be exposed to dust without the degradation of performance that is typically observed with the rigid-body mechanisms with accumulation of dust. To demonstrate the feasibility of using compliant mechanisms for EVA hardware we used the Apollo geological tool, Tongs, as an example. For this purpose, we adapted two design methods for compliant mechanisms to synthesize compliant grippers that could replace

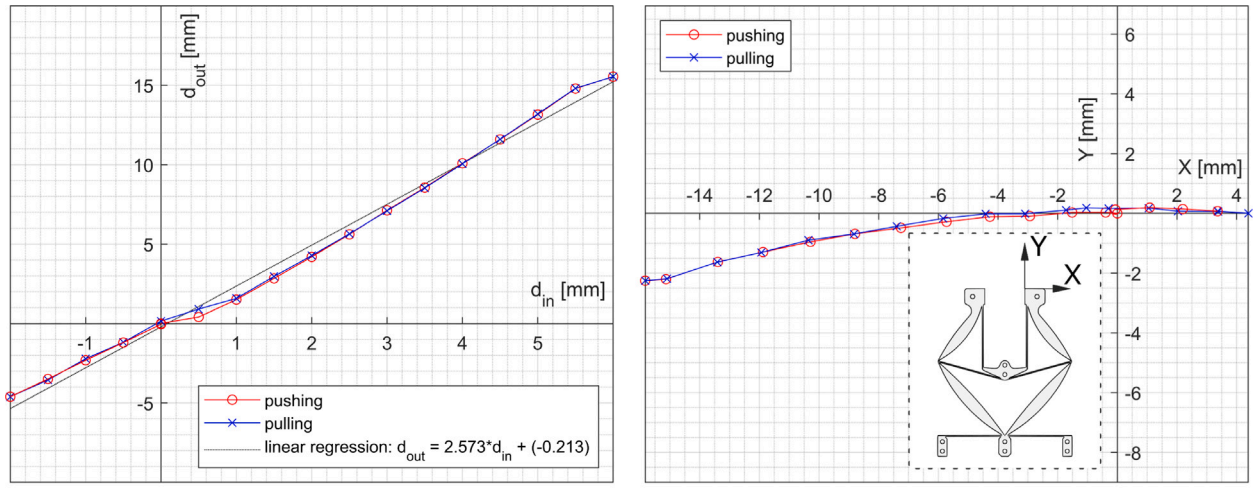

(a) Displacements relationship. (b) Output port motion path.

Fig. 15. PLA gripper kinematic behavior; graphs based on three tests and the mean of measured values; d_{in} - input displacement; d_{out} - output displacement. (For interpretation of the references to color in this figure legend, the reader is referred to the web version of this article.)

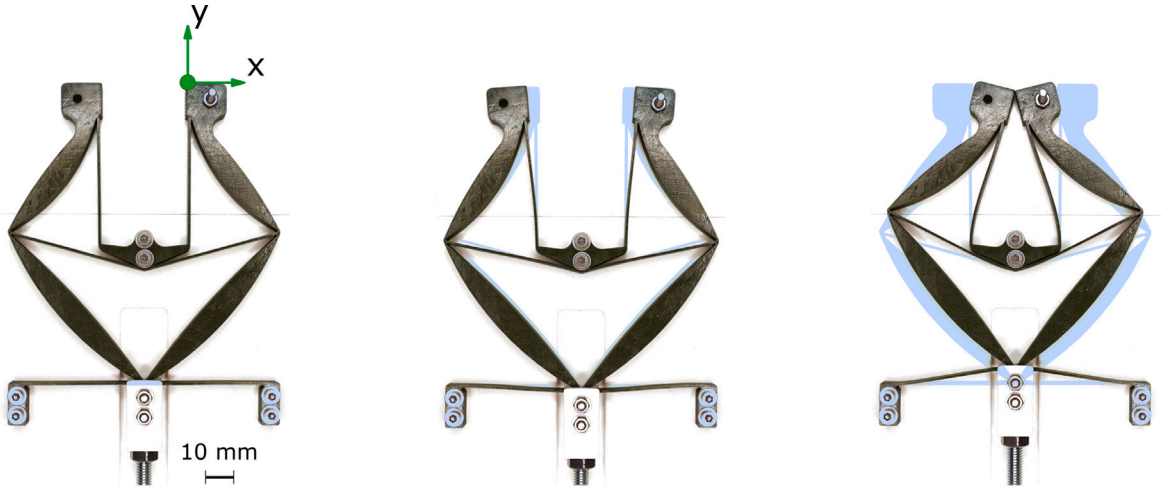

(a) Default position. (b) Open position. (c) Close position.

Fig. 16. Various deflection stages of the PLA gripper with undeformed blue shape visible in the background. (For interpretation of the references to color in this figure legend, the reader is referred to the web version of this article.)

the aforementioned tool. This case study demonstrates that compliant mechanisms represent a viable option for designing lunar hardware and can be considered for future lunar missions. The use of compliant mechanisms can minimize maintenance efforts, avoid degradation in the performance and, as demonstrated here, with appropriate design considerations replace existing traditional mechanisms. The new designs presented in this work satisfy the motion pattern expected of a gripper.

The gripper designs presented here could be used to grab objects (for example rocks) with sizes up to 40 mm. The designs are fully scalable and could be manufactured with different dimensions to target different sample sizes. The shape of the jaws affects the grasping capabilities, but it is not investigated here as it is beyond the scope of this work. Here we aim at demonstrating the suitability of complaint mechanisms for lunar EVA equipment with improved dust resilience. In addition, using 3D printed polymers could save mass, enable in-situ repair – mechanisms consisting of a single element are easy to 3D print and do not require assembly – and allow for reusability of materials which could result in a reduction of mass in future missions.

It was demonstrated that different approaches - topology optimization vs. instant center approach - result in different gripper designs, but both are valid options. This shows that compliant mechanisms can also offer a wider range of design solutions.

Another aspect worth looking at is the ratio between vertical and horizontal output displacement. For the gripper design, in general, it is preferable to have higher values of horizontal output displacement. In the case of an analytically designed gripper the ratio between vertical and horizontal output displacements is equal to 0.12. For the topologically optimized gripper this ratio is equal to 0.36. This means that the topology optimized gripper provides more motion in the vertical direction - this component of the motion does not contribute to the gripper closure. However, both grippers achieved the desired kinematic behavior: the linear input displacement achieved to open and close the gripper as desired. This work also demonstrated that there are multiple well established approaches for the synthesis of complaint mechanisms: these can support the design of the next generation of lunar EVA equipment. Our work also provides a strategy to embed implicit dust mitigation solutions at the design level, allowing for the development of hardware with improved performance for the lunar environment. The authors acknowledge that further investigations on the materials that can be used in the lunar environment and their interaction with regolith

is necessary: this is beyond the scope of this work and will be the focus of future research.

Declaration of competing interest

The authors declare that they have no known competing financial interests or personal relationships that could have appeared to influence the work reported in this paper.

Acknowledgments

This project is co-funded by the European Space Agency through ExPeRT - Exploration Preparation, Research and Technology program under the grant number ESA AO/1-10811/21/NL/MG/idb. We would like to thank ESA for supporting our research.

References

[1] B.E. Pagel, Physical properties of the lunar surface, Nature 186 (4727) (1960) 826, http://dx.doi.org/10.1038/186826b0.
[2] J.S. Levine, The Impact of Lunar Dust on Human Exploration, Cambridge Scholars Publishing, 2021.
[3] D. Rickman, K.W. Street, Some expected mechanical characteristics of lunar dust: A geological view, AIP Conf. Proc. 969 (January 2008) (2008) 949–955, http://dx.doi.org/10.1063/1.2845062.
[4] A. Abdelbary, Extreme Tribology: Fundamentals and Challenges, CRC Press, 2020.
[5] S. Pirrotta, D. Lefebvre, M.W. Co-chair, H. Wong, J. Buffington, J.J. Gaier, Dust Mitigation Gap Assessment Report, International Agency Working Group, 2016.
[6] J. Zhao, Fully kinetic particle-in-cell simulations of plasma-surface-dust interactions for lunar exploration, Missouri Univ. Sci. Technol. (2022).
[7] J.E. Colwell, S. Batiste, M. Horányi, S. Robertson, S. Sture, Lunar surface: Dust dynamics and regolith mechanics, Rev. Geophys. 45 (2) (2007) 1–26, http://dx.doi.org/10.1029/2005RG000184.
[8] J.R. Gaier, Regolith activation on the lunar surface and its ground test simulation, SAE Tech. Pap. (2009) http://dx.doi.org/10.4271/2009-01-2337.
[9] T.J. Stubbs, J.S. Halekas, W.M. Farrell, R.R. Vondrak, Lunar surface charging: A global perspective using lunar prospector data, ESA Workshop Dust Planet. Syst. (2007) 181–184.
[10] T.L. Jackson, W.M. Farrell, M.I. Zimmerman, Rover wheel charging on the lunar surface, Adv. Space Res. (2015) http://dx.doi.org/10.1016/j.asr.2014.12.027.
[11] Z. Sternovsky, S. Robertson, A. Sickafoose, J. Colwell, M. Horányi, Contact charging of lunar and martian dust simulants, J. Geophys. Res. E: Planets 107 (11) (2002) 15-1 – 15-8.
[12] D. Budzyń, E. Tuohy, N. Garrivier, T. Schild, A. Cowley, R. Cruise, M. Adachi, H. Zare-Behtash, A. Cammarano, Lunar dust: Its impact on hardware and mitigation technologies, in: 46th Aerospace Mechanisms Symposium, 2022, p. 287.
[13] J.R. Gaier, The effects of lunar dust on EVA systems during the apollo missions, 2007, Nasa/Tm-2005-213610/Rev1.
[14] t.f.N. Smithsonian, URL https://airandspace.si.edu/collection-objects/alsrc-apollo-lunar-sample-return-container-apollo-11/nasm_A197108140003. [Online; accessed 25-August-2022]. [link].
[15] P. Spanoudakis, L. Kiener, F. Cosandier, P. Schwab, L. Giriens, J. Kruis, D. Grivon, G. Psoni, C. Vrettos, N. Bencheikh, Large angle flexure pivot development for future science payloads for space applications, MATEC Web Conf. 304 (September) (2019) 07016, http://dx.doi.org/10.1051/matecconf/201930407016.
[16] L. Kiener, H. Saudan, F. Cosandier, J. Kruis, G. Perruchoud, V. Pejchal, P. Spanoudakis, J. Rouvinet, Innovative concept for additive manufacturing of compliant mechanisms, in: European Space Mechanisms and Tribology Symposium Proceedings, 2019.
[17] E.G. Merriam, J.E. Jones, S.P. Magleby, L.L. Howell, Monolithic 2 DOF fully compliant space pointing mechanism, Mech. Sci. 4 (2) (2013) 381–390, http://dx.doi.org/10.5194/ms-4-381-2013.
[18] S. Dougherty, Micro-imager dust cover, micro-imager contact sensor, and mössbauer spectrometer contact sensor mechanisms for the mars exploration rovers, in: 10th European Space Mechanisms and Tribology Symposium, Vol. 524, 2003, pp. 73–80.
[19] S. Henein, P. Spanoudakis, P. Schwab, L. Giriens, L. Lisowski, E. Onillon, L.I. Myklebust, Mechanical slit mask mechanism for the james webb space telescope spectrometer, in: J.C. Mather (Ed.), Optical, Infrared, and Millimeter Space Telescopes, Vol. 5487, SPIE, International Society for Optics and Photonics, 2004, pp. 765–776, http://dx.doi.org/10.1117/12.551106.
[20] K. Koski, Focus mechanism for Kepler mission, in: Proceedings of the 39th Aerospace Mechanisms Symposium, NASA Marshall Space Flight Center, Citeseer, 2008, pp. 359–372.
[21] W.C. Schade, Cryogenic focus mechanism for the spitzer space telescope, in: 39th Aerospace Mechanisms Symposium Proceedings, 2008, pp. 401–414.
[22] P. Spanoudakis, P. Schwab, P. Johnson, Design and production of the METOP satellite IASI corner cube mechanisms, in: 10th European Space Mechanisms and Tribology Symposium, Vol. 524, 2003, pp. 97–103.
[23] J. Budinoff, D. Pfenning, Precision linear actuators for the spherical primary optical telescope demonstration mirror, in: 38th NASA Aerospace Mechanisms Symposium, 2006.
[24] W. Coppoolse, M. Kreienbuehl, J. Moerschell, A. Dommann, D. Bertsch, Dual-axis single-mirror mechanism for beam steering and stabilisation in optical inter satellite links, in: 10th European Space Mechanisms and Tribology Symposium, Vol. 524, 2003, pp. 183–190.
[25] L.L. Howell, S.P. Magleby, B.M. Olsen, Handbook of Compliant Mechanisms, John Wiley and Sons Ltd., 2013.
[26] L. Howell, Compliant Mechanisms, in: A Wiley-Interscience Publication, Wiley, 2001.
[27] X. Zhang, B. Zhu, Topology Optimization of Compliant Mechanisms, Springer, 2018.
[28] E. Videira, C. Lebreton, S. Lewis, L. Gaillard, Guidelines for space mechanism ball-bearing design assembly and preloading operations, in: ADR, ESA and ESTL, 2013.
[29] L. Zhao, X. Yu, P. Li, Y. Qiao, High-precision compliant mechanism for lens XY micro-adjustment, Rev. Sci. Instrum. 91 (3) (2020).
[30] J. Pinskier, B. Shirinzadeh, M. Ghafarian, T.K. Das, A. Al-Jodah, R. Nowell, Topology optimization of stiffness constrained flexure-hinges for precision and range maximization, Mech. Mach. Theory 150 (2020) 103874.
[31] L. Liu, S. Bi, Q. Yang, Y. Wang, Design and experiment of generalized triple-cross-spring flexure pivots applied to the ultra-precision instruments, Rev. Sci. Instrum. 85 (10) (2014).
[32] X. Pei, J. Yu, G. Zong, S. Bi, An effective pseudo-rigid-body method for beam-based compliant mechanisms, Precis. Eng. 34 (3) (2010) 634–639.
[33] J.B. Hopkins, M.L. Culpepper, Synthesis of multi-degree of freedom, parallel flexure system concepts via freedom and constraint topology (FACT) - part I: Principles, Precis. Eng. 34 (2) (2010) 259–270.
[34] C.J. Kim, A building block approach to the conceptual synthesis of compliant mechanisms utilizing, J. Mech. Des. 130 (February) (2008) 1–11.
[35] O.M. Querin, M. Victoria, C.A. Gordoa, R. Ansola, P. Martí, Topology Design Methods for Structural Optimization, Butterworth-Heinemann, 2017.
[36] A. Saxena, G.K. Ananthasuresh, On an optimal property of compliant topologies, Struct. Multidiscip. Optim. (2000) 36–49.
[37] S. Rahmatalla, C.C. Swan, Sparse monolithic compliant mechanisms using continuum structural topology optimization, Internat. J. Numer. Methods Engrg. (2005) 1579–1605.
[38] S.R. Deepak, M. Dinesh, D.K. Sahu, G.K. Ananthasuresh, A comparative study of the formulations and benchmark problems for the topology optimization of compliant, J. Mech. Robot. 1 (1) (2009) 1–8, http://dx.doi.org/10.1115/1.2959094.
[39] M.P. Bendsoe, O. Sigmund, Topology Optimization: Theory, Methods, and Applications, Springer Science & Business Media, 2003.
[40] R. Ansola, E. Veguería, C. Alonso, O.M. Querin, Topology optimization of 3D compliant actuators by a sequential element rejection and admission method, IOP Conf. Ser.: Mater. Sci. Eng. 108 (1) (2016).
[41] L. Cao, A. Dolovich, W.J. Zhang, On understanding of design problem formulation for compliant mechanisms through topology optimization, Mech. Sci. (2013) 357–369.
[42] S. Koppen, M. Langelaar, F. van Keulen, A simple and versatile topology optimization formulation for flexure synthesis, Mech. Mach. Theory 172 (January) (2022) 104743, http://dx.doi.org/10.1016/j.mechmachtheory.2022.104743, arXiv:2111.04620.
[43] A. Klarbring, N. Strömberg, Topology optimization of hyperelastic bodies including non-zero prescribed displacements, Struct. Multidiscip. Optim. 47 (1) (2013) 37–48, http://dx.doi.org/10.1007/s00158-012-0819-z.
[44] F. Niu, S. Xu, G. Cheng, A general formulation of structural topology optimization for maximizing structural stiffness, Struct. Multidiscip. Optim. 43 (4) (2011) 561–572, http://dx.doi.org/10.1007/s00158-010-0585-8.
[45] J.H. Allton, Catalog of apollo lunar surface geological sampling tools and containers, in: NASAJJSC Solar System Exploration Division, 1989.
[46] D. Budzyn, H. Stevenin, M. Maurer, F. Sauro, L. Bessone, Prototyping of lunar surface geological sampling tools for moon spacewalk simulations by ESA, in: Proceedings of the International Astronautical Congress, IAC, Vol. 2018-Octob (October), 2018, pp. 1–5.
[47] W. Commons, File:Apollo 12 lunar hand tong (AS12-47-6932).jpg, 2022, URL https://commons.wikimedia.org/w/index.php?title=File:Apollo_12_lunar_hand_tong_(AS12-47-6932).jpg&oldid=564033943. [Online; accessed 28-July-2022].
[48] K.-J. Lu, S. Kota, Compliant mechanism synthesis for shape-change applications: Preliminary results, in: Smart Structures and Materials 2002: Modeling, Signal Processing, and Control, Vol. 4693, 2002, pp. 161–172, http://dx.doi.org/10.1117/12.475218, (June).
[49] Altair, Altair OptiStruct 2022 User Guide, Tech. rep., Altair, 2022.
[50] E. Andreassen, A. Clausen, M. Schevenels, B.S. Lazarov, O. Sigmund, Efficient topology optimization in MATLAB using 88 lines of code, Struct. Multidiscip. Optim. 43 (1) (2011) 1–16.

[51] O. Sigmund, A 99 line topology optimization code written in matlab, Struct. Multidiscip. Optim. 21 (2) (2001) 120–127.
[52] C.J. Kim, S. Kota, Y.M. Moon, An instant center approach to the conceptual design of compliant mechanisms, in: Proceedings of the ASME Design Engineering Technical Conference, Vol. 2 B, 2004, pp. 993–1005, http://dx.doi.org/10.1115/detc2004-57388.
[53] H. Li, W. Zhao, X. Wu, H. Tang, Q. Li, J. Tan, G. Wang, 3D printing and solvent dissolution recycling of polylactide-lunar regolith composites by material extrusion approach, Polymers 12 (8) (2020) http://dx.doi.org/10.3390/POLYM12081724.
[54] Spaceship EAC: 3D printing with lunar dust, 2021, URL https://blogs.esa.int/exploration/spaceship-eac-3d-printing-with-lunar-dust.